J. Fluid Mech. (1985), *vol.* 153, *pp.* 185–201
Printed in Great Britain

Nonlinear refraction–diffraction of waves in shallow water

By PHILIP L.-F. LIU, SUNG B. YOON
Joseph H. DeFrees Hydraulics Laboratory, School of Civil and Environmental Engineering, Cornell University, Ithaca, NY 14853
AND JAMES T. KIRBY†
Marine Sciences Research Center, State University of New York at Stony Brook, Stony Brook, NY 11794

(Received 11 June 1984 and in revised form 4 October 1984)

The parabolic approximation is developed to study the combined refraction/diffraction of weakly nonlinear shallow-water waves. Two methods of approach are used. In the first method Boussinesq equations are used to derive evolution equations for spectral-wave components in a slowly varying two-dimensional domain. The second method modifies the K–P equation (Kadomtsev & Petviashvili 1970) to include varying depth in two dimensions. Comparisons are made between present numerical results, experimental data (Whalin 1971) and previous numerical calculations (Madsen & Warren 1984).

1. Introduction

In recent years, recognition of the need for an improvement in the predictive capabilities of standard refraction methods (for example, Skovgaard, Jonsson & Bertelsen 1975) has led to the development of several techniques for computing wave fields modified by the combined effects of refraction and diffraction. Among these methods, the parabolic-approximation approach appears to be particularly attractive in the study of wave propagation in open coastal regions and small-angle diffraction, since its usefulness depends on a nearly unidirectional propagation of waves with little backscatter. The method was first developed for monochromatic linear waves by Radder (1979) and Lozano & Liu (1980) and has been extended to include effects such as frictional dissipation (Dalrymple, Kirby & Hwang 1984) and wave–current interaction (Booij 1981; Liu 1983; Kirby 1984). The linear model has been verified with laboratory data (Tsay & Liu 1982) and field data (Liu & Tsay 1984*a*). Liu & Tsay (1983) have also developed an iterative numerical scheme to include weak reflection. Recently, the formulation has been extended to the case of second-order Stokes waves by Yue & Mei (1980), Kirby & Dalrymple (1983) and Liu & Tsay (1984*b*).

Whalin (1971) performed a series of laboratory experiments to investigate wave focusing behind a topographical lens. Liu & Tsay (1984*b*), using the parabolic equation method, demonstrated that the Stokes second-order theory can describe adequately the wave field near the cusped caustics for cases where the Ursell number

† Present address: Department of Coastal and Oceanographic Engineering, University of Florida, Gainesville, FL 32611

is less than one; wave periods are one and two seconds in Whalin's experiment. However, for cases where the period is three seconds and the Ursell number is greater than unity, the assumptions underlying the Stokes theory become invalid. The smallness of the water depth compared to wavelength leads to a description of the wave field based on the Boussinesq equations. In Whalin's experiments, it is shown that a significant amount of wave energy is transferred from the first-harmonic component to the second and third harmonics in the focused zone, due to nonlinearity.

In this paper, we extend the parabolic-equation method to the case of nonlinear waves in shallow water. Two methods of approach are described. First, Boussinesq equations are used to derive evolution equations for spectral-wave components in a slowly varying, two-dimensional domain. Freilich & Guza (1984) have employed a similar approach to study the shoaling of nonlinear waves in one spatial direction. Secondly, we describe a similar modelling approach based on a version of the weakly two-dimensional Korteweg–de Vries equation of Kadomtsev & Petviashvili (1970) (hereinafter referred to as the K–P equation). The present approach extends the K–P equation to include varying water depth in two dimensions. The resulting systems of coupled nonlinear partial differential equations for spectral-wave components from the two approaches are quite similar. These equations are written in finite-difference form using the Crank–Nicolson method, yielding an initial-boundary-value problem for the spatial evolution of each spectral mode.

Comparisons are made between the predictions of each model and the experimental data of Whalin for the three-second case. The agreement between experimental data and numerical results is reasonable but not excellent. Both models predict much higher first-harmonic amplitudes along the centreline of the tank. The prediction for the second- and third-harmonic amplitudes seems to be better. The present model is also used to examine the refraction of a cnoidal wave over a plane slope in a rectangular channel. Numerical solutions agree very well with previous analytical and numerical results. The formation of stem waves along the boundary of the numerical wave tank is observed and discussed.

In §2 and 3, the model equations based on the Boussinesq equations and the parabolic approximation are first derived. The finite-difference forms of the resulting equations are also presented in §3. In §4, we give an alternative approach based on the K–P equation. Numerical results for Whalin's (1971) experiments are given in §5. Discussion of the refraction of cnoidal waves is presented in §6.

2. Nonlinear shallow-water wave equations

The Boussinesq equations, which include nonlinearity and dispersion to the leading order, are used as the basis of the first approach. Using ω as the characteristic frequency, a_0 as the characteristic wave amplitude and h_0 as the characteristic water depth, we introduce the following dimensionless variables:

$$\left.\begin{aligned} t = \omega t', \quad (x, y) = \frac{\omega}{(gh_0)^{\frac{1}{2}}}(x', y'), \quad z = \frac{z'}{h_0}, \\ h = \frac{h'}{h_0}, \quad \boldsymbol{u} = \boldsymbol{u}' \Big/ \left[\frac{a_0}{h_0}(gh_0)^{\frac{1}{2}}\right], \quad \zeta = \frac{\zeta'}{a_0}, \end{aligned}\right\} \tag{2.1}$$

where ζ is the free-surface displacement and $\boldsymbol{u}$ represents the depth-averaged horizontal velocity vector. The quantities with a prime denote dimensional quantities.

If the scale of the water depth is small in comparison with the horizontal lengthscale, and the wave amplitude is small compared with the water depth, i.e.

$$\mu^2 = \frac{\omega^2 h_0}{g} \ll 1, \quad \epsilon = \frac{a_0}{h_0} \ll 1, \tag{2.2a, b}$$

The Boussinesq equations take the following dimensionless forms:

$$\frac{\partial \zeta}{\partial t} + \nabla\cdot[(h+\epsilon\zeta)\,\boldsymbol{u}] = O(\epsilon^2, \epsilon\mu^2, \mu^4), \tag{2.3}$$

$$\frac{\partial \boldsymbol{u}}{\partial t} + \epsilon \boldsymbol{u}\cdot\nabla\boldsymbol{u} + \nabla\zeta = \mu^2\left\{\tfrac{1}{2}h\frac{\partial}{\partial t}\nabla[\nabla\cdot(h\boldsymbol{u})] - \tfrac{1}{6}h^2\frac{\partial}{\partial t}\nabla(\nabla\cdot\boldsymbol{u})\right\} + O(\epsilon^2, \epsilon\mu^2, \mu^4), \tag{2.4}$$

where two small parameters, ϵ and μ^2, are assumed to be of the same order of magnitude. In the present study we also assume that the variation of water depth is small in a characteristic wavelength, i.e. $O(|\nabla h|) \leqslant O(\mu^2)$.

We shall study the propagation of a shallow-water wavetrain which is periodic in time with the fundamental frequency ω. The solutions can be expressed as a Fourier series

$$\zeta(x, y, t) = \tfrac{1}{2}\sum_n \zeta_n(x, y)\,\mathrm{e}^{\mathrm{i}nt}, \quad n = 0, \pm 1, \pm 2, \ldots, \tag{2.5a}$$

$$\boldsymbol{u}(x, y, t) = \tfrac{1}{2}\sum_n \boldsymbol{u}_n(x, y)\,\mathrm{e}^{-\mathrm{i}nt}, \quad n = 0, \pm 1, \pm 2, \ldots, \tag{2.5b}$$

where $(\zeta_{-n}, \boldsymbol{u}_{-n})$ are the complex conjugates of $(\zeta_n, \boldsymbol{u}_n)$. Substituting (2.5) into (2.3) and (2.4) and collecting the coefficients of different Fourier components, we have

$$-\mathrm{i}n\zeta_n + \nabla\cdot(h\boldsymbol{u}_n) + \frac{\epsilon}{2}\sum_s \nabla\cdot(\zeta_s \boldsymbol{u}_{n-s}) = O(\epsilon^2, \epsilon\mu^2, \mu^4), \tag{2.6}$$

$$-\mathrm{i}n\boldsymbol{u}_n + \left(1 - \frac{\mu^2 n^2}{3}h\right)\nabla\zeta_n + \frac{\epsilon}{4}\sum_s (\boldsymbol{u}_s\cdot\boldsymbol{u}_{n-s}) = O(\epsilon^2, \epsilon\mu^2, \mu^4), \tag{2.7}$$

where $s = 0, \pm 1, \pm 2, \ldots$. From these two equations we can find the following simple relationships:

$$\boldsymbol{u}_n = -\frac{\mathrm{i}}{n}\nabla\zeta_n[1 + O(\epsilon, \mu^2)], \tag{2.8}$$

$$\nabla\cdot\boldsymbol{u}_n = \frac{\mathrm{i}n\zeta_n}{h}[1 + O(\epsilon, \mu^2)], \tag{2.9}$$

for $n \neq 0$, and

$$\boldsymbol{u}_0 = -\frac{\epsilon}{2h}\sum_s \zeta_s \boldsymbol{u}_{-s} + O(\epsilon^2, \mu^4, \epsilon\mu^2), \tag{2.10}$$

$$\zeta_0 = -\frac{\epsilon}{4}\sum_s \boldsymbol{u}_s\cdot\boldsymbol{u}_{-s} + O(\epsilon^2, \mu^4, \epsilon\mu^2). \tag{2.11}$$

For the case where water depth is a constant, $h = 1$, (2.6) and (2.7) reduce to those derived by Rogers & Mei (1978).

Using (2.8) and (2.9) in (2.6) and (2.7) and combining the resulting equations, we obtain

$$\nabla\cdot\left[\left(h - \frac{\mu^2 n^2 h^2}{3}\right)\nabla\zeta_n\right] + n^2\zeta_n = \frac{\epsilon}{2h}\left\{\sum_s (n^2 - s^2)\zeta_s\zeta_{n-s} - h\sum_{s\neq n}\left(\frac{n+s}{n-s}\right)\nabla\zeta_s\cdot\nabla\zeta_{n-s}\right.$$
$$\left. - 2h^2\sum_{\substack{s\neq 0\\ s\neq n}}\frac{1}{s(n-s)}\left(\frac{\partial^2\zeta_s}{\partial x^2}\frac{\partial^2\zeta_{n-s}}{\partial y^2} - \frac{\partial^2\zeta_s}{\partial x\,\partial y}\frac{\partial^2\zeta_{n-s}}{\partial x\,\partial y}\right)\right\} + O(\epsilon^2, \epsilon\mu^2, \mu^4), \tag{2.12}$$

which constitutes a system of nonlinear equations for ζ_n ($n = 1, 2, 3, \ldots$). Since (2.12) is a differential equation of the elliptic type, appropriate boundary conditions must be assigned along the boundaries. Once ζ_n ($n = 1, 2, \ldots$) are found, (2.8) can be used to calculate the velocity vector $\boldsymbol{u}_n$. The mean free-surface set-up or set-down ζ_0 is obtained from (2.11).

3. Parabolic approximation

We now consider the cases where the dominating wave propagation is known to be in the x-direction. The free-surface displacement for the nth harmonic can be written as

$$\zeta_n = \psi_n(x, y)\, \mathrm{e}^{\mathrm{i}nx} \tag{3.1}$$

where $\psi_n(x, y)$ denotes the amplitude function which takes both refraction and diffraction effects into account. Substitution of (3.1) into (2.12) yields

$$\begin{aligned} &G_n\left(\frac{\partial^2\psi_n}{\partial x^2}+\frac{\partial^2\psi_n}{\partial y^2}\right)+\left(2\mathrm{i}nG_n+\frac{\partial G_n}{\partial x}\right)\frac{\partial\psi_n}{\partial x}+\frac{\partial G_n}{\partial y}\frac{\partial\psi_n}{\partial y}+\left(\mathrm{i}n\frac{\partial G_n}{\partial x}-n^2G_n+n^2\right)\psi_n \\ &\quad=\frac{\epsilon}{2h}\Bigg\{\sum_s\left[hs(n+s)+(n^2-s^2)\right]\psi_s\psi_{n-s} \\ &\quad\quad-h\sum_{s\neq n}\left(\frac{n+s}{n-s}\right)\left[\nabla\psi_s\cdot\nabla\psi_{n-s}+\mathrm{i}s\psi_s\frac{\partial\psi_{n-s}}{\partial x}+\mathrm{i}(n-s)\psi_{n-s}\frac{\partial\psi_s}{\partial x}\right] \\ &\quad\quad-2h^2\sum_{\substack{s\neq 0\\ s\neq n}}\frac{1}{s(n-s)}\Bigg[\frac{\partial^2\psi_s}{\partial x^2}\frac{\partial^2\psi_{n-s}}{\partial y^2}-\frac{\partial^2\psi_s}{\partial x\,\partial y}\frac{\partial^2\psi_{n-s}}{\partial x\,\partial y}-s^2\psi_s\frac{\partial^2\psi_{n-s}}{\partial y^2} \\ &\quad\quad+s(n-s)\frac{\partial\psi_s}{\partial y}\frac{\partial\psi_{n-s}}{\partial y}+\mathrm{i}\left(2s\frac{\partial\psi_s}{\partial x}\frac{\partial^2\psi_{n-s}}{\partial y^2}-s\frac{\partial\psi_s}{\partial y}\frac{\partial^2\psi_{n-s}}{\partial x\,\partial y}-(n-s)\frac{\partial^2\psi_s}{\partial x\,\partial y}\frac{\partial\psi_{n-s}}{\partial y}\right)\Bigg]\Bigg\} \\ &\quad\quad+O(\mu^4, \epsilon\mu^2, \epsilon^2), \end{aligned} \tag{3.2}$$

where

$$G_n = h-\frac{\mu^2n^2h^2}{3}. \tag{3.3}$$

In principle (3.2) can be solved as a system of boundary-value problems for ψ_n.

The amplitude function ψ_n is primarily a function of the water depth due to wave shoaling. Therefore, ψ_n varies slowly in the direction of wave propagation at the same rate as that of h in the x-direction. Thus,

$$\frac{\partial\psi_n}{\partial x}\sim\frac{\partial h}{\partial x}\sim O(\epsilon, \mu^2), \quad \frac{\partial^2\psi_n}{\partial x^2}\sim O(\epsilon^2, \mu^4, \epsilon\mu^2). \tag{3.4a, b}$$

The diffraction effects are considered important. Hence

$$\frac{\partial\psi_n}{\partial y}\sim O(1). \tag{3.4c}$$

Using (3.4), we can simplify (3.2) significantly:

$$\begin{aligned} &2\mathrm{i}n\frac{\partial\psi_n}{\partial x}+\frac{\partial^2\psi_n}{\partial y^2}+\frac{1}{G_n}\frac{\partial G_n}{\partial y}\frac{\partial\psi_n}{\partial y}+\left[\frac{\mathrm{i}n}{G_n}\frac{\partial G_n}{\partial x}-n^2\left(1-\frac{1}{G_n}\right)\right]\psi_n \\ &\quad=\frac{\epsilon}{2hG_n}\Bigg\{\sum_s\left[hs(n+s)+n^2-s^2\right]\psi_s\psi_{n-s}-h\sum_{s\neq n}\left(\frac{n+s}{n-s}\right)\frac{\partial\psi_s}{\partial y}\frac{\partial\psi_{n-s}}{\partial y} \\ &\quad\quad+2h^2\sum_{s\neq n}\frac{1}{n-s}\left[s\psi_s\frac{\partial^2\psi_{n-s}}{\partial y^2}-(n-s)\frac{\partial\psi_s}{\partial y}\frac{\partial\psi_{n-s}}{\partial y}\right]\Bigg\}. \end{aligned} \tag{3.5}$$

More importantly, we have converted a set of elliptic equations (3.2) into a set of parabolic equations (3.5) which may be solved with efficient numerical techniques. For later use, we can rewrite (3.5) in a dimensional form

$$2ink_0'\frac{\partial\psi_n'}{\partial x'}+\frac{1}{\bar{G}_n}\frac{\partial}{\partial y'}\left(\bar{G}_n\frac{\partial\psi_n'}{\partial y'}\right)+\frac{1}{\bar{G}_n}\left(ink_0'\frac{\partial\bar{G}_n}{\partial x'}-n^2k_0'^2\bar{G}_n+\frac{n^2\omega^2}{g}\right)\psi_n'$$

$$=\frac{1}{\bar{G}_n}\left\{\tfrac{1}{2}\sum_s\left[k_0'^2s(n+s)+\frac{\omega^2}{gh'}(n^2-s^2)\right]\psi_s'\psi_{n-s}'-\tfrac{1}{2}\sum_{s\neq n}\left(\frac{n+s}{n-s}\right)\frac{\partial\psi_s'}{\partial y'}\frac{\partial\psi_{n-s}'}{\partial y'}\right.$$

$$\left.+\sum_{s\neq n}\frac{gk_0'^2h'}{\omega^2(n-s)}\left[s\psi_s'\frac{\partial^2\psi_{n-s}'}{\partial y'^2}-(n-s)\frac{\partial\psi_s'}{\partial y'}\frac{\partial\psi_{n-s}'}{\partial y'}\right]\right\}, \tag{3.6}$$

where

$$\bar{G}_n=h'\left(1-\frac{n^2\omega^2h'}{3g}\right) \tag{3.7}$$

is the dimensional form of (3.3) and

$$k_0'=\frac{\omega}{(gh_0')^{\frac{1}{2}}} \tag{3.8}$$

is the wavenumber associated with a reference constant water depth h_0'. The model equation (3.5) provides a means for calculating the evolution of either a single wavetrain containing a fundamental frequency and its harmonics, as in the subsequent examples, or of a broad spectrum of waves, where the fundamental frequency is taken to be the lowest mode in the spectrum. The current results thus extend the analysis of Freilich & Guza (1984) to two horizontal dimensions, and allow for the modelling of wavetrains with a small but non-trivial directional spreading about the principal propagation direction.

The Crank–Nicolson method is used to rewrite the governing differential equations (3.5) in a finite-difference form. The forward-difference scheme is employed in the x-direction, which is a time-like variable, and a centred-difference scheme is used in the y-direction. Denoting $\psi_{n,j}^m$ as the nth harmonic function at x $(=m\Delta x)$ and y $(=j\Delta y)$, we can write (3.5) in the following form:

$$2in\frac{\psi_{n,j}^{m+1}-\psi_{n,j}^m}{\Delta x}+\frac{\delta^2\psi_{n,j}^{m+1}+\delta^2\psi_{n,j}^m}{2(\Delta y)^2}+\left(\frac{1}{G_n}\frac{\partial G_n}{\partial y}\right)_j^{m+1}\left(\frac{\delta\psi_{n,j}^{m+1}+\delta\psi_{n,j}^m}{4\Delta y}\right)$$

$$+\left[\frac{in}{G_n}\frac{\partial G_n}{\partial x}-n^2\left(1-\frac{1}{G_n}\right)\right]_j^{m+1}\left(\frac{\psi_{n,j}^{m+1}+\psi_{n,j}^m}{2}\right)$$

$$=\frac{\epsilon}{2h_j^{m+1}G_{n,j}^{m+1}}\left\{\tfrac{1}{2}\sum_s\left[h_j^{m+1}s(n+s)+(n^2-s^2)\right](\psi_{s,j}^{m+1}\psi_{n-s,j}^{m+1}+\psi_{s,j}^m\psi_{n-s,j}^m)\right.$$

$$-h_j^{m+1}\sum_{s\neq n}\left(2h_j^{m+1}+\frac{n+s}{n-s}\right)\left(\frac{\delta\psi_{s,j}^{m+1}\delta\psi_{n-s,j}^{m+1}+\delta\psi_{s,j}^m\delta\psi_{n-s,j}^m}{8(\Delta y)^2}\right)$$

$$\left.+(h_j^{m+1})^2\sum_{s\neq n}\frac{s}{n-s}\left[\psi_{s,j}^{m+1}\frac{\delta^2\psi_{n-s,j}^{m+1}}{(\Delta y)^2}+\psi_{s,j}^m\frac{\delta^2\psi_{n-s,j}^m}{(\Delta y)^2}\right]\right\}, \tag{3.9}$$

where

$$\delta^2\psi_{n,j}^m=\psi_{n,j+1}^m-2\psi_{n,j}^m+\psi_{n,j-1}^m, \tag{3.10}$$

$$\delta\psi_{n,j}^m=\psi_{n,j+1}^m-\psi_{n,j-1}^m. \tag{3.11}$$

The right-hand side of (3.9) is nonlinear in terms of ψ^{m+1}. We linearize the nonlinear terms by adopting an iterative procedure as follows:

$$\psi_{s,j}^{m+1}\psi_{n-s,j}^{m+1}=\begin{cases}(\psi_{s,j}^{m+1})^k(\psi_{n-s,j}^{m+1})^{k+1}, & \text{if } s<0,\ n-s>0,\\ (\psi_{s,j}^{m+1})^{k+1}(\psi_{n-s,j}^{m+1})^k, & \text{otherwise,}\end{cases} \tag{3.12}$$

where the superscripts $k+1$ and k denote the current and previous iterations respectively. The initial guesses, $k=0$, are obtained from the previous x-level solutions, i.e. $(\psi_{n,j}^{m+1})^0 = \psi_{n,j}^m$. The iteration procedure is stopped and converged solutions are obtained when the relative error between two successive iteration solutions is less than a predetermined small number δ i.e.

$$\frac{|(\psi_{n,j}^{m+1})^{k+1} - (\psi_{n,j}^{m+1})^k|}{|(\psi_{n,j}^{m+1})^k|} < \delta. \tag{3.13}$$

In our present calculations, the value of δ is chosen as 10^{-4}.

4. An alternative approach based on the K–P equation

The application of the parabolic approximation to the more general Boussinesq equations involves an implied restriction to the case of waves with a unidirectional propagation direction and small transverse modulation. In this connection, it is of some interest to examine model equations with time dependence incorporated which embody the same basic assumption. For the case of shallow water and constant depth, an equation of this form has been developed by Kadomtsev & Petviashvili (1970). The K–P equation may be written (following Bryant 1982) as

$$\frac{\partial}{\partial x}\left(\frac{\partial \zeta}{\partial t}+\frac{\partial \zeta}{\partial x}+\frac{3\epsilon}{2}\zeta\frac{\partial \zeta}{\partial x}+\frac{\mu^2}{6}\frac{\partial^3 \zeta}{\partial x^3}\right)+\frac{1}{2}\frac{\partial^2 \zeta}{\partial y^2} = O(\epsilon^2, \epsilon\mu^2, \mu^4). \tag{4.1}$$

The connection to the parabolic approximation may be seen by considering only $O(1)$ terms and making the substitution

$$\zeta = \psi(x, y)\, e^{i(x-t)}, \tag{4.2}$$

yielding (after assuming $O(\partial^2\psi/\partial x^2) \ll O(\partial\psi/\partial x)$)

$$2i\frac{\partial \psi}{\partial x}+\frac{\partial^2 \psi}{\partial y^2} = 0, \tag{4.3}$$

which is the parabolic approximation of the Helmholtz equation (Yue & Mei 1980). The K–P equation, which extends the Korteweg–de Vries equation to include weak transverse modulation, thus contains the same degree of information as the parabolic approximation.

Based on this correspondence, we may construct a version of the K–P equation for variable depth. Retaining dimensional quantities, the resulting model equation may be written as

$$\frac{\partial}{\partial x'}\left(\frac{1}{C'}\frac{\partial \zeta'}{\partial t'}+\frac{\partial \zeta'}{\partial x'}+\frac{1}{4h'}\frac{\partial h'}{\partial x'}\zeta'+\frac{3}{2h'}\zeta'\frac{\partial \zeta'}{\partial x'}+\frac{(h')^2}{6}\frac{\partial^3 \zeta'}{\partial x'^3}\right)+\frac{1}{2h'}\frac{\partial}{\partial y'}\left(h'\frac{\partial \zeta'}{\partial y'}\right) = 0, \tag{4.4}$$

where $C' = (gh')^{\frac{1}{2}}$. Neglecting y derivatives, the equation reduces to the form given by Johnson (1972) after non-dimensionalization. Retaining only lowest-order terms, making the substitution

$$\zeta' = \bar{\psi}(x', y')\, e^{i(\int k'\,dx' - \omega t')}, \quad \omega = C'k', \tag{4.5a, b}$$

and referencing the phase function to a constant value k_0' (following Kirby & Dalrymple 1983) leads to the parabolic approximation

$$2ik'h'\frac{\partial \psi'}{\partial x'}+2k'h'(k'-k_0')\psi'+i\frac{\partial (k'h')}{\partial x'}\psi'+\frac{\partial}{\partial y'}\left(h'\frac{\partial \psi'}{\partial y'}\right) = 0, \tag{4.6}$$

which is simply the shallow-water limit of the linear approximation,

$$2ik'C'C'_g\frac{\partial\psi'}{\partial x'}+2k'C'C'_g(k'_0-k')\,\psi'+i\frac{\partial}{\partial x'}(k'C'C'_g)\,\psi'+\frac{\partial}{\partial y'}\left(C'C'_g\frac{\partial\psi'}{\partial y'}\right)=0, \quad (4.7)$$

obtained by Kirby & Dalrymple (1983). In (4.7) $C'_g=\partial\omega/\partial k'$ is the group velocity.

Before substituting a series expansion for ζ', it is advantageous to alter the dispersive term $\partial^3\zeta'/\partial x'^3$ by the following substitution:

$$\frac{\partial^2\zeta'}{\partial t'^2}-g\frac{\partial}{\partial x'}\left(h'\frac{\partial\zeta'}{\partial x'}\right)=O(\epsilon,\mu^2),$$

yielding the modified equation

$$\frac{\partial}{\partial x'}\left\{\frac{1}{C'}\frac{\partial\zeta'}{\partial t'}+\frac{\partial\zeta'}{\partial x'}+\frac{1}{4h'}\frac{\partial h'}{\partial x'}\zeta'+\frac{3}{2h'}\zeta'\frac{\partial\zeta'}{\partial x'}\right\}+\frac{h'}{6C'^2}\frac{\partial^3}{\partial t'^2\partial x'}\left(h'\frac{\partial\zeta'}{\partial x'}\right)+\frac{1}{2h'}\left(h'\frac{\partial\zeta'}{\partial y'}\right)=0, \quad (4.8)$$

which has the same dispersion relation as (2.3) and (2.4). The parabolic approximation is obtained in similar fashion to the procedure of §§2 and 3; we proceed using the slightly revised form

$$\zeta'=\frac{1}{2}\sum_{n=-\infty}^{\infty}\bar{\psi}'_n(x',y')\,e^{in(\int k'\,dx'-\omega t')}, \quad (4.9)$$

to manipulate (4.8) initially, after which a shift to a reference depth is employed (as in (4.6)) to obtain

$$2ink'_0\frac{\partial\psi'_n}{\partial x'}+\frac{k'_0}{k'\bar{G}_n}\frac{\partial}{\partial y'}\left(h'\frac{\partial\psi'_n}{\partial y'}\right)+\frac{1}{\bar{G}_n}\left[\frac{ink'_0}{2}\frac{\partial\bar{G}_n}{\partial x'}-2n^2k'_0(k'_0-k')\,\bar{G}_n+\frac{n^4}{3}\left(\frac{k'_0}{k'}\right)\frac{\omega^4h'}{g^2}\right]\psi'_n$$
$$=\frac{3n^2k'k'_0}{4\bar{G}_n}\left[\sum_{s=1}^{n-1}\psi'_s\psi'_{n-s}+2\sum_{s=1}^{N-n}\psi'_{-s}\psi'_{n+s}\right], \quad 1\leqslant n\leqslant N \quad (4.10)$$

where

$$\zeta'=\frac{1}{2}\sum_{n=-\infty}^{\infty}\psi'_n(x',y')\,e^{in(k'_0x'-\omega t')} \quad (4.11)$$

and where $\bar{G}_n$ and k'_0 are given in (3.7) and (3.8) respectively. The difference in the coefficients of ψ'_n in (3.6) and (4.10) is accounted for by the fact that the substitution (4.11) is used throughout the entire process to obtain (3.6) rather than the intermediate form (4.9).

Comparing (4.10) with the corresponding equation (3.6), derived from the Boussinesq equation, we observe that the basic characteristics of these equations are the same. We note, however, that in the approach using the K–P equation the nonlinearity is localized due to the original form of the equation (no y-derivatives) in nonlinear terms, and that the retention of only the lowest-order depth dependence in the y-derivative term implies a possible error in energy-flux conservation for wave shoaling over a general two-dimensional topography. It seems from (3.6) and (4.10) that this effect could be alleviated by making the substitution $\partial(\bar{G}_n\,\partial\psi'_n/\partial y')/\partial y'$ for the given term. Several numerical experiments using the revised term have indicated that this is not a significant effect in present computations.

The parabolic equation (4.10) can be solved numerically in similar fashion as that presented in the previous section for (3.5). Only slight changes in the coefficients and the right-hand side of (3.9) are required. The details are not repeated here.

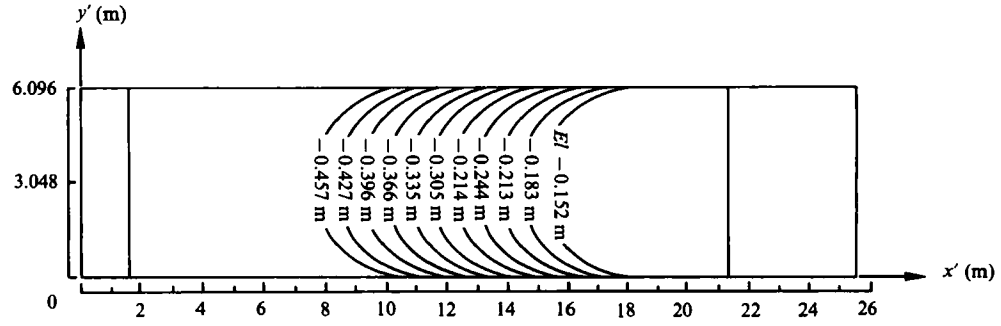

FIGURE 1. Topographical lens in Whalin's (1971) wave–tank experiments.

Wave period T (s)	Incident-wave amplitude a_0 (cm)			$\epsilon = a_0/h_1$			$\mu^2 = \omega^2 h_1/g$
3.0	0.68	0.98	1.46	0.0446	0.0643	0.0958	0.0682

TABLE 1. Experimental and numerical parameters

5. Wave focusing by a topographical lens

Whalin (1971) conducted a series of laboratory experiments concerning wave convergence over a bottom topography that acts as a focusing lens. The wave tank used in the experiments has the horizontal dimensions 25.603 m × 6.096 m. In the middle portion of the wave tank, 7.62 m < x' < 15.24 m, eleven semicircular steps were evenly spaced and led to the shallower portion of the channel (figure 1). The equations approximating the topography are given as follows (Whalin, 1971):

$$h'(x', y') = \begin{cases} 0.4572 & (0 \leqslant x' < 10.67 - G(y')), \\ 0.4572 + \frac{1}{25}(10.67 - G - x'), & (10.67 - G \leqslant x' \leqslant 18.29 - G), \\ 0.1524 & (18.29 - \mathrm{G} \leqslant x' \leqslant 21.34), \end{cases} \tag{5.1}$$

where

$$G(y') = [y'(6.096 - y')]^{\frac{1}{2}} \quad (0 \leqslant y' \leqslant 6.096). \tag{5.2}$$

In both (5.1) and (5.2) the length variables are measured in metres. The bottom topography is symmetric with respect to the centreline of the wave tank, $y' = 3.048$ m.

A wavemaker was installed at the deeper portion of the channel where the water depth h_0' is 0.4572 m. Three sets of experiments were conducted by generating waves with periods $T = 1$, 2, and 3 s. Different wave amplitudes were generated for each wave period. For the cases of $T = 1$ and 2 s, a second-order Stokes-wave theory has been shown to describe the combined refraction–diffraction mechanisms adequately (Liu & Tsay 1984*b*). The focusing of water waves by refraction led to a focal region, in which energy was transferred to the second harmonic. For the experimental set with $T = 3$ s, the Ursell parameter $U_r = (a/h)/(kh)^2$ is generally greater than unity in the shallower-water region, which indicates that the Stokes-wave theory is no longer valid and the present shallow-water wave theory should be used. In table 1,

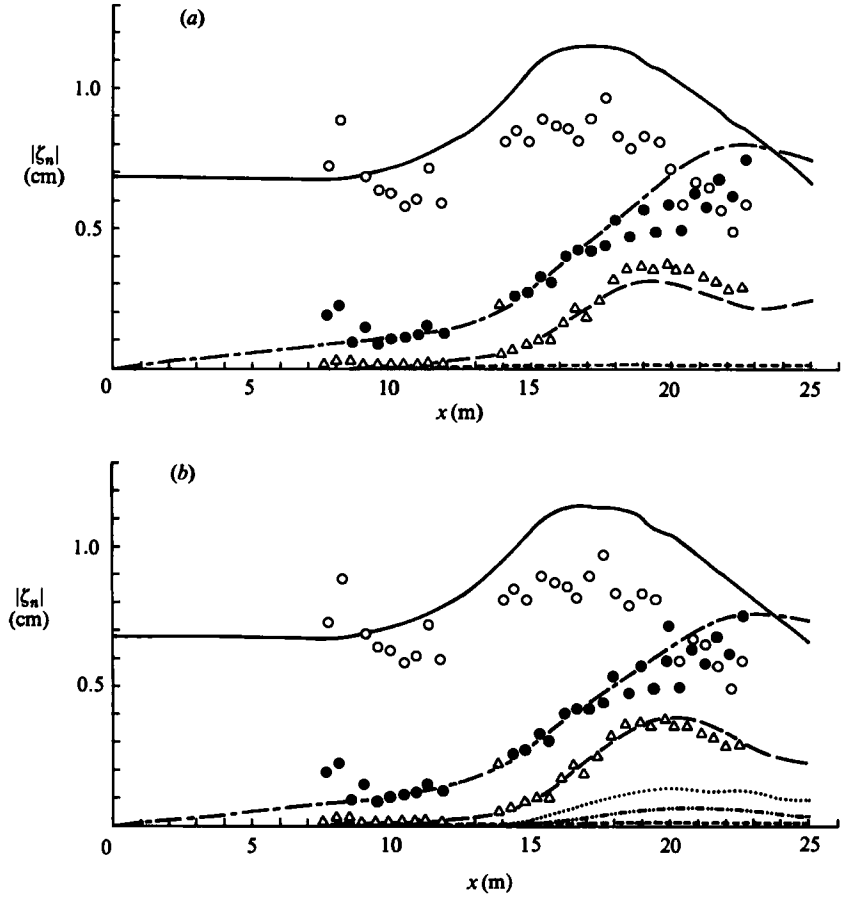

FIGURE 2. Wave amplitudes along the centreline of the wave tank for $a_0 = 0.68$ cm, $\epsilon = 0.0446$, and $\mu^2 = 0.0682$. Numerical results (experimental data): —— (○○○), first harmonic; ——— (●●●), second harmonic; ——— (△△△), third harmonic; ·····, fourth harmonic; —·—, fifth harmonic; and ----, mean free surface.

we summarize the experimental data and the corresponding small parameters ϵ and μ^2. The water depth in the shallower region, $h_1' = 0.1524$ m, has been used as the water-depth scale.

According to the Whalin's report, the second- and the third-harmonic waves grow rapidly in the focal zone. In fact, the amplitude of the higher harmonics becomes larger than that of the first harmonic (see figures 2, 3 and 4). To study this problem, we obtain numerical solutions by using both approaches (3.5) and (4.10). In numerical computations for each model, three harmonics ($N = 3$) and five harmonics ($N = 5$) are considered.

Owing to the symmetry of the problem with respect to the centreline of the wave tank, only one half of the wave tank is discretized. The computational domain starts from the wavemaker, $x' = 0$, and ends at $x' = 25$ m. The no-flux boundary conditions are used along the side-wall and the centreline of the wave tank, i.e.

$$\frac{\partial \psi_n'}{\partial y'} = 0, \quad \text{along } y' = 0 \text{ and } 3.048 \text{ m}, \tag{5.3}$$

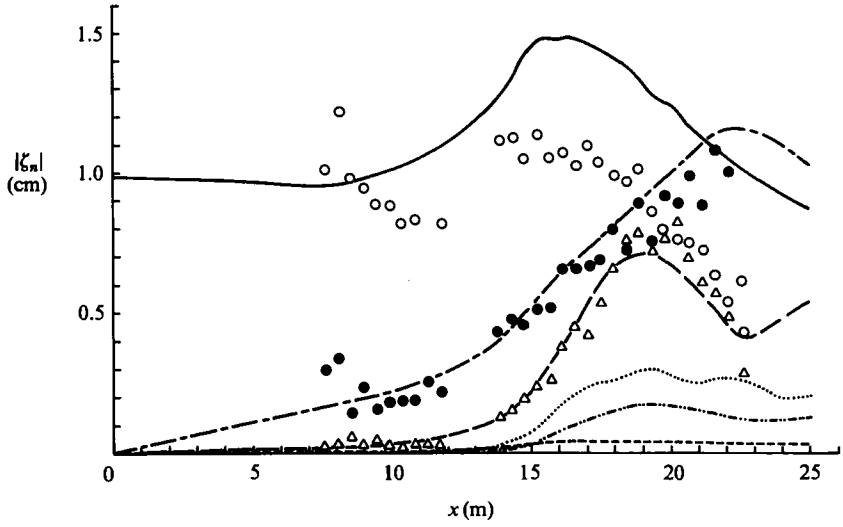

FIGURE 3. Wave amplitudes along the centreline of the wave tank for $a_0 = 0.98$ cm, $\epsilon = 0.0643$, and $\mu^2 = 0.0682$; see figure 2 caption for symbols.

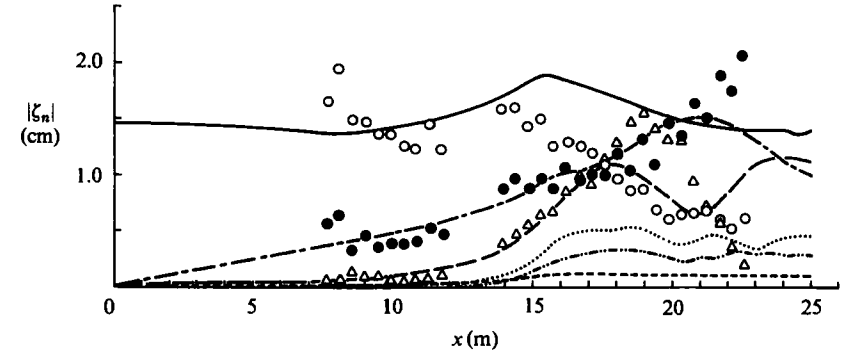

FIGURE 4. Wave amplitudes along the centreline of the wave tank for $a_0 = 1.46$ cm, $\epsilon = 0.0958$, and $\mu^2 = 0.0682$; see figure 2 caption for symbols.

for all n. The wave amplitude for the first-harmonic waves at the wavemaker ($x' = 0$) is prescribed with the values shown in table 1. The initial conditions for higher-harmonic waves are zero.

In numerical computations different grid sizes are tested for the convergence of the numerical scheme. Numerical solutions presented here are obtained by using $\Delta x' = 0.25$ m and $\Delta y' = 0.3048$ m, although no noticeable differences are observed when the grid sizes are doubled. Less than five iterations are necessary to satisfy the convergency condition (3.13) at each x'.

In figure 2, numerical results based on the Boussinesq equations approach (3.5) for the case with $\epsilon = 0.0446$, $\mu^2 = 0.0682$ and $a_0 = 0.0068$ m are presented with experimental data. Wave amplitudes along the centreline of the wave tank are plotted; figure 2(a) contains three harmonics and figure 2(b) represents numerical results with five harmonics. Since it is assumed that only the first-harmonic waves are generated at the wavemaker, the wave energy in the higher-harmonic components are sufficiently small over the constant-depth region ($0 < x' < 8$ m). However, as

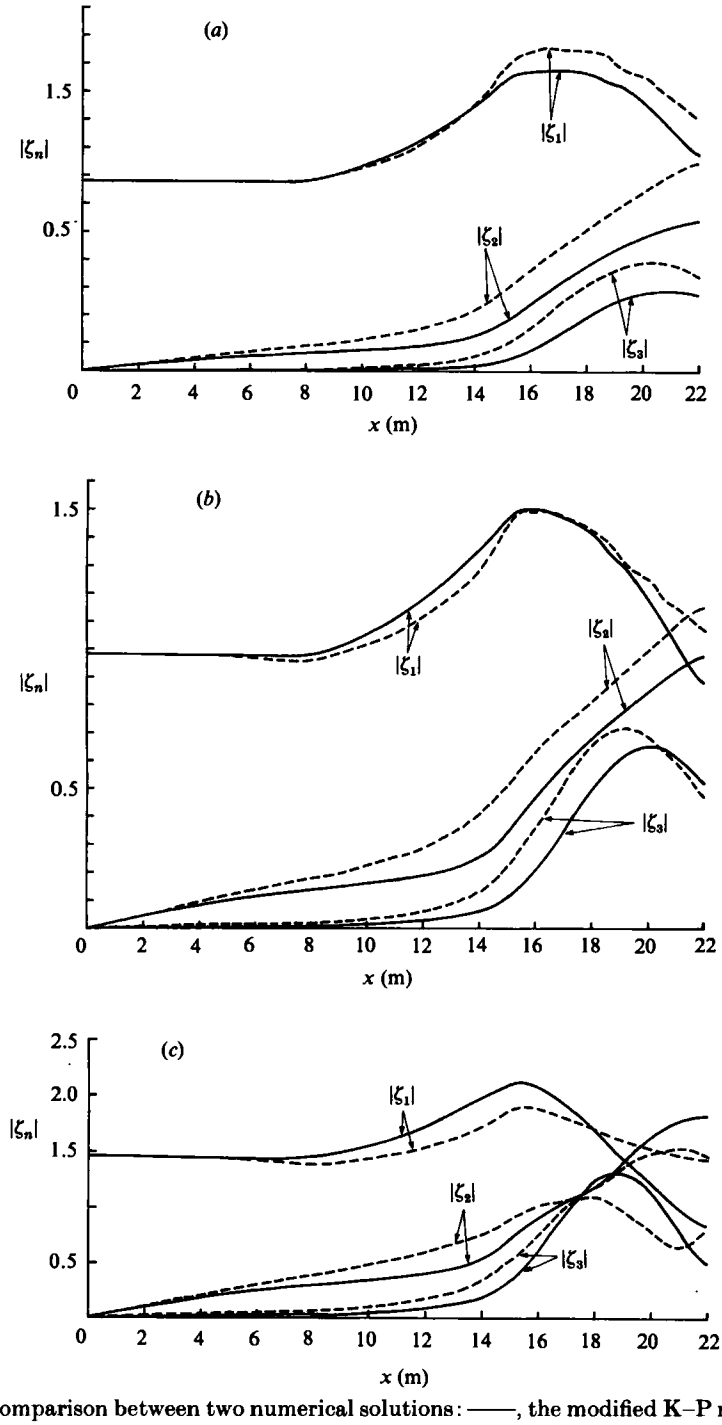

FIGURE 5. Comparison between two numerical solutions: ——, the modified K–P model (4.10); and – – – –, Boussinesq model (3.5); (*a*) $a_0 = 0.68$ cm, $\mu^2 = 0.0682$, and $\epsilon = 0.0446$, (*b*) $a_0 = 0.98$ cm, $\mu^2 = 0.0682$, and $\epsilon = 0.0446$, and (*c*) $a_0 = 1.46$ cm, $\mu^2 = 0.0682$, and $\epsilon = 0.0958$.

waves start to refract over the topography and focus along the centreline of the tank, a significant amount of energy is transferred into higher-harmonic components. The agreement between laboratory data and numerical solutions is reasonable. The numerical model overestimates the first-harmonic amplitudes. The second- and third-harmonic wave amplitudes are in good agreement with reported data. Keeping more harmonic components in the analysis seems to reduce the amplitudes in the first two harmonics slightly and increase the third-harmonic amplitudes. The agreement between laboratory data and numerical results is improved if more higher-harmonic components are included.

The difference in results for low-harmonic amplitudes apparent in figure 2 indicates the importance of retaining sufficient harmonics to obtain convergence of the low-mode solutions. For this reason the choice $N = 5$ was retained for the remainder of the calculations in this section. (Several experiments with higher values of N indicated only minor changes for modes 1–3). Results for the cases $a_0 = 0.0098$ m ($\epsilon = 0.0643$, $\mu^2 = 0.0682$) and $a_0 = 0.0146$ m ($\epsilon = 0.0958$, $\mu^2 = 0.0682$) are shown in figures 3 and 4 respectively. Again, the model uniformly overpredicts first-harmonic amplitude along the channel centreline, although the amplitude of the second-harmonic is well predicted in both cases. The third-harmonic amplitude is also well predicted in figure 3. This high-amplitude case of figure 4 indicates a tendency for the numerical result to undergo the start of a recurrence behaviour before the experimental maximum of ζ_3 is obtained.

Numerical results for the three cases presented above were also obtained using the K–P model (4.10) with $N = 5$. To compare these two models, numerical solutions for the first three harmonics are shown in figure 5(*a–c*). For the low-amplitude case $a_0 = 0.68$ cm (figure 5*a*), the results from the K–P model show an underprediction of second- and third-harmonic amplitudes in comparison to the Boussinesq.† For the higher-amplitude cases (figure 5*b* and *c*), nonlinearity becomes relatively more important and results of the two models are in closer agreement, with the exception that harmonic amplitudes grow somewhat more slowly in the K–P model. Both models are seen to be capable of predicting the essential features of harmonic generation in the focusing of a nonlinear wave. We note that the results of each model are sensitive to the choice of initial conditions, so that more detailed comparisons than those obtained here are not possible in the absence of detailed data in the vicinity of the wavemaker ($x < 8$ m).

The discrepancy between theory and experiment in the amplitude of the first harmonic could be partially caused by frictional dissipation on the waves. Whalin (1971) reported that there is a very small amount of wave damping (roughly 3 %) owing to the viscous boundary layers along the sidewalls and the bottom of the wave tank; in our numerical computations viscous damping has been ignored. The other contributing factor to the disagreement is that the evolution process described by the experiment occurs in the space of about two first-harmonic wavelengths, indicating that the theoretical limitation to slowly varying amplitudes is not truly satisfied. On the other hand, reasonable agreement between theory and experiment also suggests that the assumption concerning slowly varying amplitudes is not restrictive in practice.

† This discrepancy appears to be the results of slightly different frequency dispersion effects at $O(\mu^2)$ between the two models.

6. Refraction of waves over a plane slope

The results in the preceding section have demonstrated successfully the present models' ability to predict the transfer of energy to harmonic components during the process of nonlinear focusing. However, measured and predicted amplitudes of the fundamental component were markedly different along the channel centreline, indicating either erroneous predictions by the model or some inconsistency in Whalin's reported data. For this reason, it was desirable to compare the present models' results with some case for which analytic results are available. Such a case has been provided by Skovgaard & Peterson (1977), who used the properties of a very slowly varying train of cnoidal waves to develop a theory for the refraction and shoaling of obliquely incident waves on a plane beach. This situation has also been studied recently by Madsen & Warren (1984), who obtained a numerical solution for the case of waves propagating in a rectangular channel containing a plane slope oriented at an angle of 26.6° to the channel sidewalls. Madsen & Warren used a time-dependent, finite-difference solution of a set of conservation laws equivalent to (2.3) and (2.4) to obtain their numerical results. Here, we use the parameters chosen by Madsen & Warren and study the same channel configuration; however, we neglect the lateral boundary damping employed by Madsen & Warren in order to study the details of the reflection process at the vertical, impermeable sidewalls. The computational domain is given by $0 \leqslant x' \leqslant 2154.5$ m, $0 \leqslant y' \leqslant 1534.5$ m, with waves normally incident at $x = 0$. Slope-oriented coordinates are given by

$$\left.\begin{aligned} \bar{x} &= (x'-420)\cos(26.6°)-(y'-775)\sin(26.6°),\\ \bar{y} &= (x'-420)\sin(26.6°)+(y'-775)\cos(26.6°), \end{aligned}\right\} \tag{6.1}$$

with water depth given by

$$h'(\bar{x},\bar{y}) = \begin{cases} 21 \text{ m}, & \bar{x} < 0,\\ (21-0.013\,\bar{x})\text{ m}, & 0 \leqslant \bar{x} \leqslant 1076.9 \text{ m},\\ 7 \text{ m}, & \bar{x} > 1076.9 \text{ m}. \end{cases} \tag{6.2}$$

Wave parameters for the problem are given by:

$$T = 17.3 \text{ s} = \text{wave period};$$

$$H = 1.74 \text{ m} = \text{wave height at 21 m depth};$$

which gives a deep-water wavelength $L_0 = 467.1$ m and an Ursell number $U_r = (H/2h')/(k'h')^2 = 0.13$ in the deep-water portion of the channel. Initial conditions for the calculation are thus specified according to a third-order Stokes wave at $x = 0$. A total of $N = 6$ components are retained, and the computational domain is divided into a rectangular grid with either $\Delta x' = \Delta y' = 15.5$ m or $\Delta x' = \Delta y' = 10.0$ m. The larger grid spacing is used to be consistent with that used by Madsen & Warren ($\Delta x' = \Delta y' = 15.5$ m). The smaller grid spacing is used to eliminate plotting errors when reproducing the narrow wave crests. Wave heights calculated using the larger grid spacing agree in detail with previous numerical computations.

A plot of the model topography is given in figure 6 along with a photograph of the instantaneous water-surface elevation, with contour increments of 1 m for bottom topography and 0.4 m for surface elevation. As the wave shoals, refraction effects are apparent in the centre of the channel, and the wave develops from nearly sinusoidal form to shallow-water profiles with narrow crests and broad troughs. The formulation

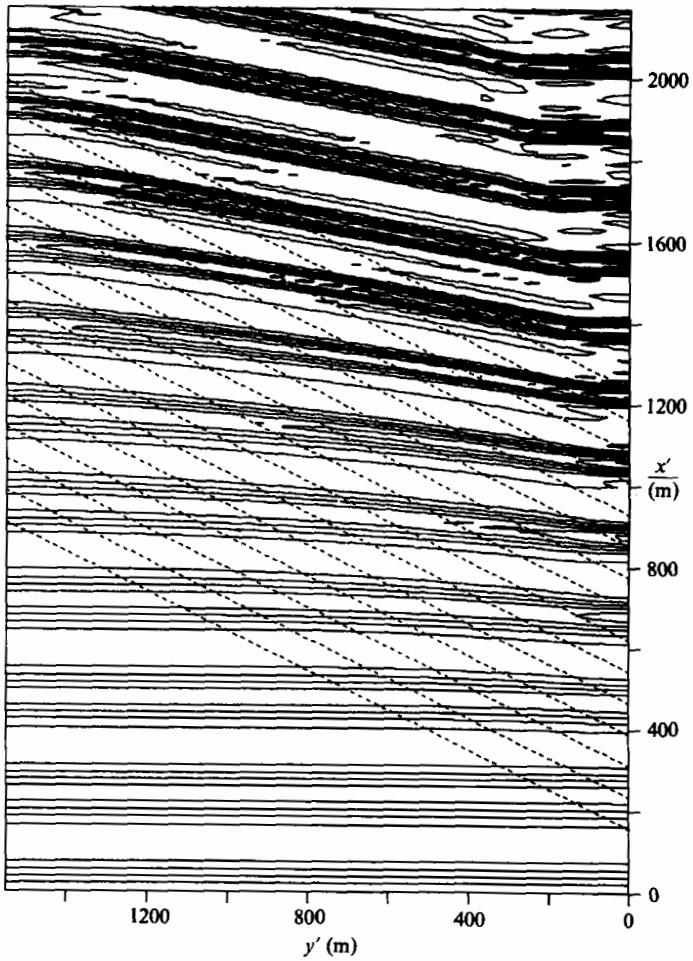

FIGURE 6. Bottom topography and contours of instantaneous surface elevation at $t = 0$; ----, bottom contours in increments of 1 m, 7 m $< h <$ 21 m; ——, contours of free-surface elevation in increments of 0.4 m.

of a 'Mach stem' is apparent on the fifth boundary, where refraction turns the incident wave towards the wall, inducing a grazing-incidence reflection as in the study of Yue & Mei (1980). Some high-frequency modulation along the wave crests appears due to the combined effect of plotter error and numerical discretization; this modulation is significant for the choice $\Delta x' = \Delta y' = 15.5$ m but disappears rapidly with decreasing grid spacing.

A plot of normalized wave height H/h versus normalized water depth h/L_0 for $y' = 750$ m is given in figure 7 in comparison with the refraction model of Skovgaard & Peterson (1977) and the time-dependent numerical results of Madsen & Warren (1984). These results were obtained using $\Delta x' = \Delta y' = 15.5$ m, in agreement with Madsen & Warren's calculations. The evolution of H/h is seen to be quite smooth up to the shallower depths, with the plotted points (corresponding to every fifth computational point) agreeing quite well with the refraction theory. In the shallow portion of the tank, some modulation of the local wave height is present, possibly due to interaction with the lateral boundaries. Wave height H was obtained by

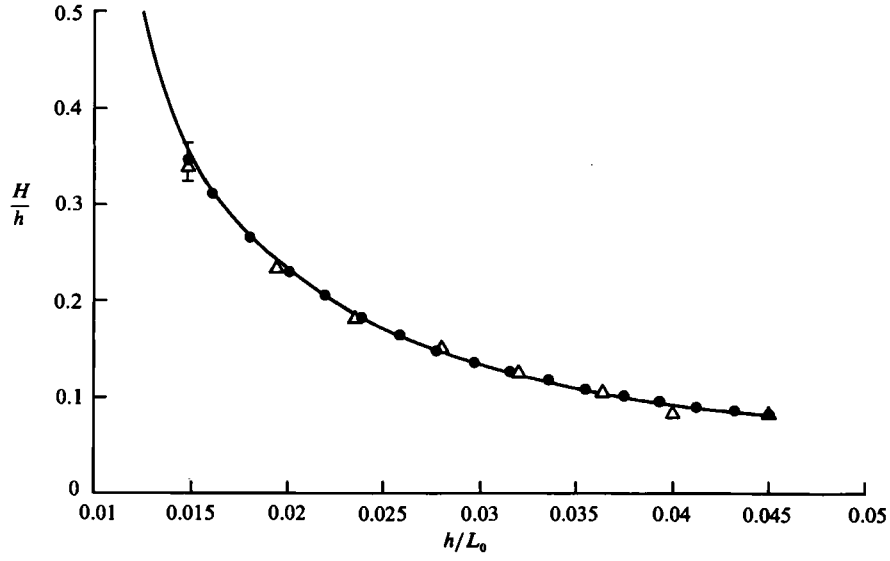

FIGURE 7. Normalized waveheight H/h as a function of h/L_0: ——, refraction results of Skovgaard & Peterson (1977); △△△, numerical results of Madsen & Warren (1984); . . ., present numerical results. Error bar ♀ at $h/L_0 = 0.015$ indicates range of H values in shallow part of tank due to short-wave modulation.

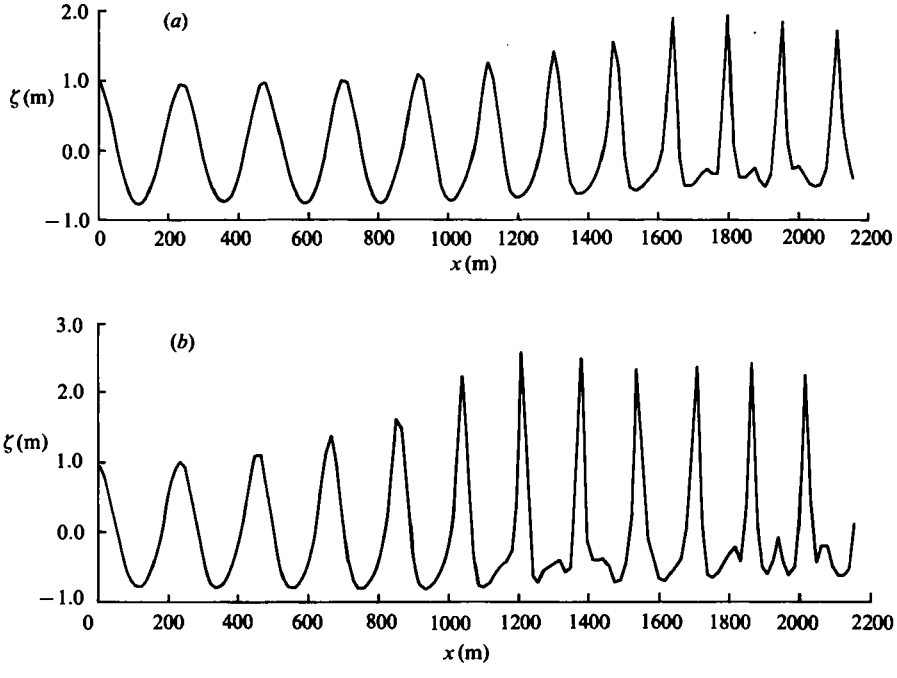

FIGURE 8. Free-surface profiles for cnoidal wave refraction: (*a*) along $y = 750$ m, near the centreline of channel and (*b*) along $y = 0$ m, sidewall and through 'Mach-stem' region.

stepping the individual components through time to construct $\zeta'(x', y', t')$ and then taking $H(x', y')$ to correspond to $\zeta'_{\max} - \zeta'_{\min}$, a crest-to-trough measure.

Refracted angles of incidence between the wave and slope also agreed quite well with the refraction model and are not shown.

Plots of the water-surface profile along the line $y' = 750$ m and through the 'Mach-stem' region $y' = 0$ m are shown in figure 7 (*a* and *b*). In both cases, the results show the presence of separate peaks in the wave troughs. This effect was also noted in the results of Madsen & Warren and was attributed by them to the effect of truncation errors, although no physical evidence exists to exclude their possible physical existence. The rapid evolution of a nearly uniform wavetrain is evident in the 'Mach-stem' region in figure 6. We note that, due to the narrowness of the wave crests, displacement of these crests away from actual computational grid points may contribute significantly to the modulation of crest elevations $\zeta'_{\max}$ which is apparent in the plotted results.

7. Concluding remarks

The present study has demonstrated that the parabolic equation method may be applied successfully to the modelling of weakly nonlinear, weakly dispersive wave motions governed by the Boussinesq equations. The present study has been confined to the investigation of the propagation of monochromatic waves together with their nonlinearly generated harmonics. However, given the necessary computer capacity, the method is directly applicable to the problem of modelling two-dimensional spectral evolution in shallow water.

In this study we have neglected the effects of frictional dissipation and wave breaking; the models in their present form are thus applicable to the region seaward of the surf zone. The inclusion of wave-breaking effects in the models may be expected to be a non-trivial extension of the present results, since the models do not directly calculate the total wave height at each computational point.

The model developed here could be used for modelling an entire spectrum of wave motion, thus extending the work of Freilich & Guza (1984) to two horizontal dimensions. Computer times required are likely to be large but may be manageable on standard computers for simulations involving less than one hundred spectral components, using a revised form of iteration for the nonlinear terms, which decouples the Crank–Nicolson step for each equation.

This research was carried out with the support of New York Sea Grant Institute (PLFL and SBY) and the Office of Naval Research, Coastal Sciences Program (JTK). The possible utility of the K–P equation in the study of combined refraction and diffraction was suggested by Dr J. L. Hammack. Dr D. H. Peregrine's comments on the earlier version of the paper are also acknowledged.

REFERENCES

Booij, N. 1981 Gravity waves on water with non-uniform depth and current. *Rep.* 81–1, *Dept. Civil Engng, Delft University of Technology.*

Bryant, P. J. 1982 Two-dimensional periodic permanent waves in shallow water. *J. Fluid Mech.* **115**, 525–532.

Dalrymple, R. A., Kirby, J. T. & Hwang, P. A. 1984 Wave diffraction due to areas of energy dissipation. *J. Waterway, Port, Coastal and Ocean Engineering, ASCE* **110**, 67–79.

FREILICH, M. H. & GUZA, R. T. 1984 Nonlinear effects on shoaling surface gravity waves. *Phil. Trans. R. Soc. Lond.* **A311**, 1–41.

JOHNSON, R. S. 1972 Some numerical solutions of a variable-coefficient Korteweg–de Vries equation (with applications to solitary wave development on a shelf). *J. Fluid Mech.* **54**, 81–91.

KADOMTSEV, B. B. & PETVIASHVILI, V. I. 1970 On the stability of solitary waves in weakly dispersing media. *Sov. Phys. Dokl.* **15**, 539–541.

KIRBY, J. T. 1984 A note on linear surface wave–current interaction over slowly varying topography. *J. Geophys. Res.* **89**, 745–747.

KIRBY, J. T. & DALRYMPLE, R. A. 1983 A parabolic equation for the combined refraction–diffraction of Stokes waves by mildly varying topography. *J. Fluid Mech.* **136**, 453–466.

LIU, P. L.-F. 1983 Wave–current interactions on a slowly varying topography. *J. Geophys. Res.* **88**, 4421–4426.

LIU, P. L.-F. & TSAY, T.-K. 1983 On weak reflection of water waves. *J. Fluid Mech.* **131**, 59–71.

LIU, P. L.-F. & TSAY, T.-K. 1984*a* Numerical prediction of wave transformation. *J. Waterway, Port, Coastal and Ocean Engrg. Div. ASCE.* (to appear).

LIU, P. L.-F. & TSAY, T.-K. 1984*b* Refraction–diffraction model for weakly nonlinear water waves. *J. Fluid Mech.* **141**, 265–274.

LOZANO, C. & LIU, P. L.-F. 1980 Refraction–diffraction model for linear surface water waves. *J. Fluid Mech.* **101**, 705–720.

MADSEN, P. A. & WARREN, I. R. 1984 Performance of a numerical short-wave model. *Coastal Engng* **8**, 73–79.

RADDER, A. C. 1979 On the parabolic equation method for water-wave propagation. *J. Fluid Mech.* **95**, 159–176.

ROGERS, S. R. & MEI, C. C. 1978 Nonlinear resonant excitation of a long and narrow bay. *J. Fluid Mech.* **88**, 161–180.

SKOVGAARD, O., JONSSON, I. G. & BERTELSEN, J. A. 1975 Computation of wave heights due to refraction and friction. *J. Waterways, Port, Harbors and Coastal Engng Div., ASCE* **101**, 15–32.

SKOVGAARD, O. & PETERSEN, H. M. 1977 Refraction of cnoidal waves. *Coastal Engng* **1**, 43–61.

TSAY, T.-K. & LIU, P. L.-F. 1982 Numerical solution of water-wave refraction and diffraction problems in parabolic approximation. *J. Geophys. Res.* **87**, 7932–7940.

WHALIN, R. W. 1971 The limit of applicability of linear wave refraction theory in a convergence zone. *Res. Rep.* H-71-3, *U.S. Army Corps of Engrs, Waterways Expt. Station, Vicksburg, MS.*

YUE, D. K. P. & MEI, C. C. 1980 Forward diffraction of Stokes waves by a thin wedge. *J. Fluid Mech.* **99**, 33–52.